


Article

Modeling Wildfire Spread with an Irregular Graph Network

Wenyu Jiang ^{1,2} , Fei Wang ^{1,2,*}, Guofeng Su ¹, Xin Li ³, Guanning Wang ¹, Xinxin Zheng ^{1,2}, Ting Wang ^{1,2} and Qingxiang Meng ⁴

¹ Department of Engineering Physics, Tsinghua University, Beijing 100084, China

² Institute of Safety Science and Technology, Tsinghua Shenzhen International Graduate School, Shenzhen 518000, China

³ Foshan Urban Safety Research Center, Foshan 528000, China

⁴ School of Remote Sensing and Information Engineering, Wuhan University, Wuhan 430000, China

* Correspondence: feiwang@tsinghua.edu.cn

Abstract: The wildfire prediction model is crucial for accurate rescue and rapid evacuation. Existing models mainly adopt regular grids or fire perimeters to describe the wildfire landscape. However, these models have difficulty in explicitly demonstrating the local spread details, especially in a complex landscape. In this paper, we propose a wildfire spread model with an irregular graph network (IGN). This model implemented an IGN generation algorithm to characterize the wildland landscape with a variable scale, adaptively encoding complex regions with dense nodes and simple regions with sparse nodes. Then, a deep learning-based spread model is designed to calculate the spread duration of each graph edge under variable environmental conditions. Comparative experiments between the IGN model and widely used fire simulation models were conducted on a real wildfire in Getty, California, USA. The results show that the IGN model can accurately and explicitly describe the spatiotemporal characteristics of the wildfire spread in a novel graph form while maintaining competitive simulation refinement and computational efficiency (Jaccard: 0.587, SM: 0.740, OA: 0.800).



Citation: Jiang, W.; Wang, F.; Su, G.; Li, X.; Wang, G.; Zheng, X.; Wang, T.; Meng, Q. Modeling Wildfire Spread with an Irregular Graph Network. *Fire* **2022**, *5*, 185. <https://doi.org/10.3390/fire5060185>

Academic Editor: Chad M. Hoffman

Received: 9 September 2022

Accepted: 2 November 2022

Published: 4 November 2022

Publisher's Note: MDPI stays neutral with regard to jurisdictional claims in published maps and institutional affiliations.



Copyright: © 2022 by the authors. Licensee MDPI, Basel, Switzerland. This article is an open access article distributed under the terms and conditions of the Creative Commons Attribution (CC BY) license (<https://creativecommons.org/licenses/by/4.0/>).

Keywords: wildfire spread; irregular graph network; variable scale; deep learning; emergency rescue

1. Introduction

Wildfires are some of the most serious natural hazards in the world, affecting the earth's surface and atmosphere for over 350 million years and causing significant loss of life, along with economic and ecological effects [1,2]. In 2019, forest fires in Australia, lasting nearly 6 months, burned almost 8 million acres and killed at least 28 people [3]. Large-scale wildfires directly destroy vegetation and threaten wildlife while releasing large amounts of gases that affect humans in the long term [4–6]. Modeling wildfire spread is crucial to ensure the accurate deployment of firefighting resources and to conduct prompt, targeted evacuation and avoid wildland firefighter entrapments [7,8].

Wildfire spread models can be summarized as empirical and quasi-empirical [9], physical and quasi-physical [10], or as simulation and mathematical analogs [11]. Empirical models use experimental data to construct empirical functions of environmental parameters and fire spread rates [12–16]. Due to the experimental parameters being typically applicable only to specific scenarios, the empirical model may fail to accurately reflect wildfire spread under scenarios that differ substantially from their basis. Inherently different from empirical models, physical models quantify the wildfire spread process in terms of thermal conduction, convection, and radiation based on thermodynamic theory [17–20]. The physical characteristic makes the universality of physical models superior to empirical models. However, purely physical simulation is computation-intensive with a time-consuming iterative solution process, making them difficult to simulate wildfire in the large-scale wildland with high timeliness. To address the above issues, mathematical analog models are constructed by mathematical equations and physical mechanisms. These models

have higher timeliness and maintain competitive accuracies [21–23], such as the Huygens model [24–26] and the cellular automata (CA) model [27–31]. As a vector-based method, the Huygens model discretizes the fire perimeter into a series of independent fire ignitions, calculates the perimeter of the next time step at each ignition by an empirical elliptical model, and fuses these perimeters to form a new fire perimeter. Rothermel [23] proposed a mathematical fire model for predicting the rate of spread and intensity and further implemented the BEHAVE fire prediction system [32,33]. Based on the Rothermel model, vector-based ellipse models were constructed to simulate the fire spread from a single ignition point [34,35]. Finney [36,37] proposed a fire simulation model named FARSITE based on the Huygens method, including fire behavior models for surface, crown, spotting, point-source fire acceleration, and fuel moisture. The simulation accuracy of the Huygens model depends on the refinement of perimeter discretization, and the calculation process is fairly complex and requires computational resources. In contrast, the grid-based cellular automata model is gaining momentum due to its simple structure and low computational complexity [28–30,38–40]. This model divides the wildfire landscape into a series of regular, contiguous cells and constructs a state transition function f to determine the moment when a cell is ignited under its neighborhood conditions. Then a minimum travel time algorithm [41] is implemented to iteratively calculate the ignition time of each cell from the ignition. The landscape division method is crucial for these grid-based models since it greatly determines the design of the transition function f . Most landscapes of CA models are divided into regular quadrilaterals [29,30], and some are hexagonal [42,43]. These regular grids usually have the same spatial resolution; therefore, an appropriate resolution is important since a higher resolution needs more computation and storage, while a lower resolution results in poor refinement in a complex landscape. For instance, when the wildfire landscape is highly heterogeneous, a regular grid may contain various fuels and variable slopes, which increases the uncertainty of cell properties and even causes significant simulation bias. It is natural to consider increasing the spatial resolution to reduce the grid heterogeneity. However, this will exponentially increase computational requirements and data storage space. In addition, the output formats of Huygens and CA models are fire perimeter and regular grids, respectively. These formats are difficult to explicitly demonstrate the spatiotemporal details of wildfire spread, such as the spread route.

The graph network, consisting of a series of nodes and edges, has been an important model for characterizing the complex physical world [44–47]. This graph structure has the advantage of describing the relationship between graph nodes and contains the potential to demonstrate the spread details of wildfire. Compared to regular grids, the graph network is more flexible and can, therefore, adaptively characterize complex landscapes and even some abstract social relationships. For example, the triangulated irregular network, as a special graph network, has been widely used to characterize geographic topology, with a refined grid for complex regions and a coarse grid for simple regions so as to save storage [47,48]. In wildfire research, the random configuration graph was proposed to analyze the association of graph node distribution patterns and predict the number of surviving trees after a fire [49,50]. Graph networks were adopted to analyze the association between fire suppression nodes and firefighter deployment and survival [51–53]. As for the wildfire spread prediction, Johnston [54] proposed irregular grids to minimize the distortion of fire shapes brought by the grid-based model. However, the nodes of irregular grids are generated by a random distribution, and simulation results were presented with the fire perimeters instead of irregular grids. Stepanov [55] then used the Delaunay triangulation to represent the landscape and evaluate the rate of fire spread along any edge. Hajian [56] represented the landscape as a graph network and modeled the fire propagation time as the stochastic shortest path problem. However, the triangulation generation of these models is relatively complex, as it ensures that polygons have constant properties in terms of fuel and topography, but the fire spreads along graph edges instead of polygons. In addition, the rate of spread is calculated by the elliptical fire model, which has a certain complexity

in the computational solution. Other important wildfire behaviors for firefighters, such as flame length and fire intensity [57], are also neglected in these models.

Inspired by deep learning [58–62], the graph network is gaining momentum with the deep neural network (DNN) and forms the graph convolutional network (GCNs), which have been applied to characterize physical surfaces and simulate physical deformations under external forces [63–65]. Different from traditional mathematical models, DNN can be defined as a combination of multiple nonlinear layers $Y = DNN(X)$. For each layer ($y = \sigma(xA^T + b)$), the input x is first processed by a linear layer ($v = xA^T + b$), where the A^T and b are the linear transformation matrix and the bias matrix, respectively. The linear output v is then mapped into a nonlinear space by an activation layer ($y = \sigma(v)$). Then, the output y of this nonlinear layer is taken as the input x of the next nonlinear layer. Here, A^T and b are model parameters and randomly initialized. The back-propagating learning approach [66] is a crucial component of DNN, as it is able to update the model parameters A^T and b of each layer by the gradient information in back propagation. Therefore, DNN has the ability to learn data features autonomously, reducing the large amount of manual feature design work in traditional methods. The universal approximation theorem of DNN has been proved by Hecht [67], and many complex applications have demonstrated the competitive accuracy and efficiency of the data-driven DNN model [68–71]. Therefore, it would be a good choice to adopt DNN to model the wildfire spread in the graph network.

In this paper, we propose a wildfire spread model with an irregular graph network (IGN) to simulate and analyze the spatiotemporal spread of wildfires in a variable-scale landscape. An IGN generation algorithm adaptively adjusts the graph node density according to the landscape complexity, enabling the variable-scale homogeneity of graph nodes and edges. Valid spread nodes (VSNs) and valid spread edges (VSEs) are defined to describe the wildfire spread process in the special IGN. Then, a deep learning-based spread model is implemented to calculate the spread time, flame length, and fire intensity from the ignited nodes to the unignited nodes. A real wildfire, the Getty fire in California, United States (US), was selected as the study case, and comparative results with the widely used FARSITE model and CA model were conducted. The results show that the IGN model can explicitly demonstrate the spatiotemporal spread of wildfires in the graph landscape with a competitive performance in simulation refinement and computational efficiency.

The remainder of this paper is organized as follows: we introduce our materials and methods in Section 2. Section 3 describes our experimental results, Section 4 presents the discussion analysis, and Section 5 is the conclusion.

2. Materials and Methods

2.1. Experimental Area

To demonstrate and validate our IGN model, we chose a real wildfire named Getty Fire as a study case, which occurred in California, US, on 28 October 2019. This wildfire broke out at 01:34:00 and spread for nearly 10 h until it was almost completely controlled by firefighters. Detailed records can be found in the Los Angeles Fire Department [72]. The fire ignition was located at $34^{\circ}5'47''$ N, $118^{\circ}28'53''$ W and the burned area of the final fire perimeter was about 704 acres. We followed the details in [27] to collect and process model data from LANDFIRE [73], USGS [74], and Mesowest [75]. The wildfire region and dynamic weather data are shown in Figure 1. Comparative experiments are conducted with the widely used FARSITE model [36] and CA model [27]. These three models are representative in the field of wildfire spread prediction and differ in theoretical principle, spread pattern, landscape type, and output format, as Appendix A illustrates. In addition, we should note that spot fire was a nonlinear and stochastic fire behavior [76–79]. There was the possibility that the spot fire had occurred in the Getty Fire. However, any record of the spot fire in the Getty Fire was not found. Given the stochasticity and the lack of records, spot fire was not taken into account in current models.

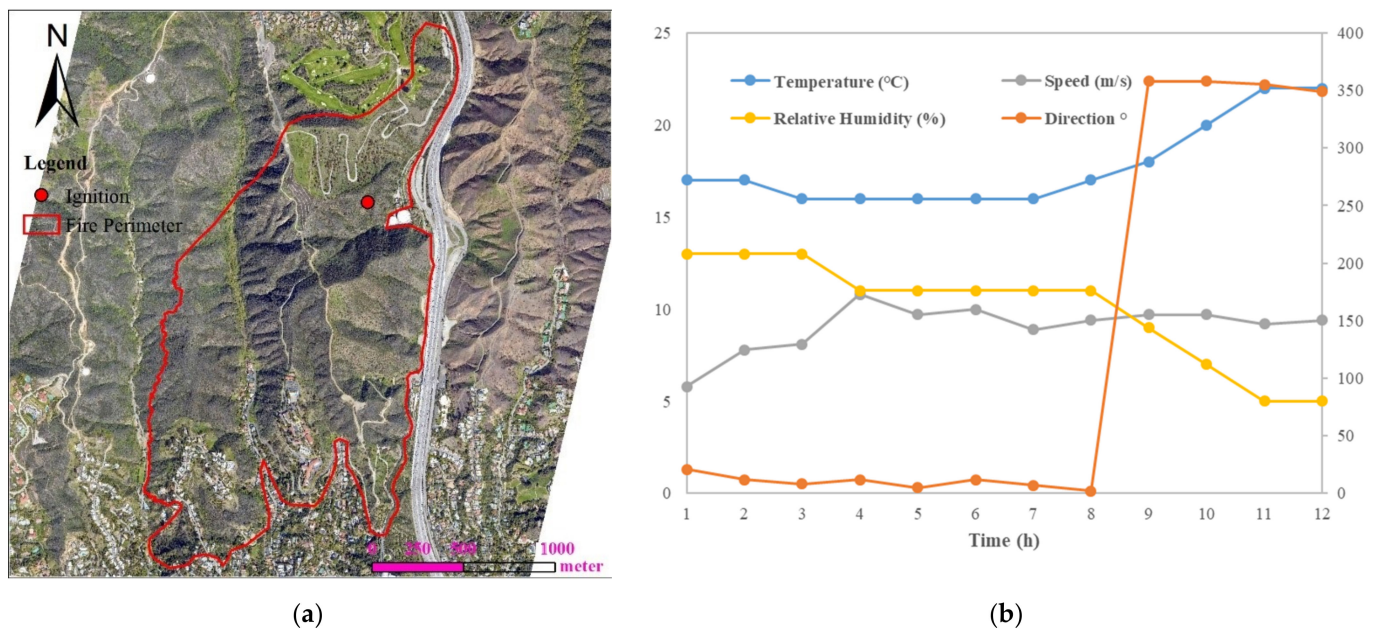


Figure 1. Study case in Getty Fire. (a) Wildfire region; (b) historical weather data.

All models were executed on the same hardware equipment, a 4-core (2.30 GHz) Inter(R) Core (TM) i7-10510U laptop with 16 GB of RAM. The final perimeter of Getty Fire was taken as the baseline to quantitatively evaluate the simulation results of the above three models. The perimeter was measured by both GPS tracker and remote sensing imagery on November 2nd, and the wildfire was totally controlled by firefighters at that time. Many evaluation metrics have been proposed to measure the similarity between the predictive wildfires and the actual wildfire perimeters [76,77]. Here, we adopted the Sorensen metric (SM) [76], Jaccard coefficient [77], and overall accuracy (OA) [78] to quantitatively evaluate model performance, as shown in Equations (1)–(3).

$$Sorensen = \frac{2 \cdot TP}{2 \cdot TP + FP + FN'} \tag{1}$$

$$Jaccard = \frac{TP}{TP + FP + FN'} \tag{2}$$

$$OA = \frac{TP + TN}{TP + FP + FN + TN'} \tag{3}$$

where TP is the true positive rate (number of predictions s_1 with corresponding labels s_1 , where s_1 is the burned area, s_0 is the unburned area), TN is the true negative rate (number of predictions s_0 with corresponding labels s_0), FP is the false positive rate (number of predictions s_1 with corresponding labels s_0), and FN is the false negative rate (number of predictions s_0 with corresponding labels s_1). As the output format of the IGN model is a graph, the simulation result of the IGN model cannot be directly applied to the above metrics. Therefore, a kriging interpolation algorithm was used to convert the graph nodes into a raster map. Then the region within 600 min is extracted and further compared with the recorded perimeter.

In addition to the above three metrics, the recorded burned area at a different time of the Getty Fire [72] was collected, and an area metric was set to compare the real burned area with the predicted areas by these models. The burned areas were recorded at 111, 171, 191, 216, 281, 406, and 446 min. Therefore, the area metric was defined as the average area error (AAE) of these moments. Additionally, model runtime was also adopted as an important metric to analyze the model’s computational efficiency.

2.2. Variable-Scale Landscape with IGN

2.2.1. Definition of the IGN

When there are various fuels or variable slopes on a graph edge, it indicates the heterogeneity problem. To address this problem, we implement an IGN generation algorithm to characterize the wildfire landscape with a variable scale. Different from the previous graph method [54–56], this generation algorithm directly aims at ensuring that graph edges have constant properties in terms of fuel and topography instead of polygons. The density and distribution of graph nodes are adaptively adjusted according to the landscape complexity. First, we use $G = (V, E)$ to define the IGN and then elaborate on its basic components, graph nodes V , and graph edges E . Each graph node $node^i \in V$ represents a dimensionless independent cell with the properties,

$$A_{node} = \{ID, X, Y, Fuel, Elevation, Time\}, \tag{4}$$

where ID is the unique code of the graph node, (X, Y) are geographic coordinates, $Fuel$ is the fuel type; here, we adopt the fuel model in the FARSITE model to classify the fuel type [36]. $Elevation$ is the absolute elevation, and $Time$ is set to record the ignition time of each node and initialized to infinity. The graph edge $edge^i \in E$ describes the connection properties between graph nodes,

$$A_{edge} = \{ID_{start}, ID_{target}, Fuel, Slope, Length, Angle\}, \tag{5}$$

where ID_{start} and ID_{target} are unique codes for the start and target node in a graph edge, respectively. $Slope$ is the edge slope (from ID_{start} to ID_{target}), determined by the edge length $Length$ and elevation of two graph nodes. $Angle$ is the azimuth angle, describing the direction of the vector formed by ID_{start} and ID_{target} , within a range of $0-2\pi$. After defining the property space, IGN initialization and optimization are introduced to determine the spatial distribution of the graph nodes.

2.2.2. IGN Initialization

As shown in Figure 2, we set the maximum graph resolution GR_{max} and the minimum graph resolution GR_{min} . The GR_{max} is the shortest edge length in the IGN while the GR_{min} is the longest length. Uniform sampling with distance interval GR_{min} is adopted to initialize the spatial distribution of graph nodes. The Delaunay algorithm [79,80] is adopted to construct graph edges based on the spatial distribution of graph nodes. The edge property A_{edge} is critical to wildfire spread simulation as it determines the rate of spread. However, edge properties are likely to be heterogeneous and cannot be accurately defined; various fuel or variable slope may exist in a graph edge when the landscape is complex. Therefore, it is necessary to optimize the spatial distribution of graph nodes to ensure the homogeneity of graph edges.

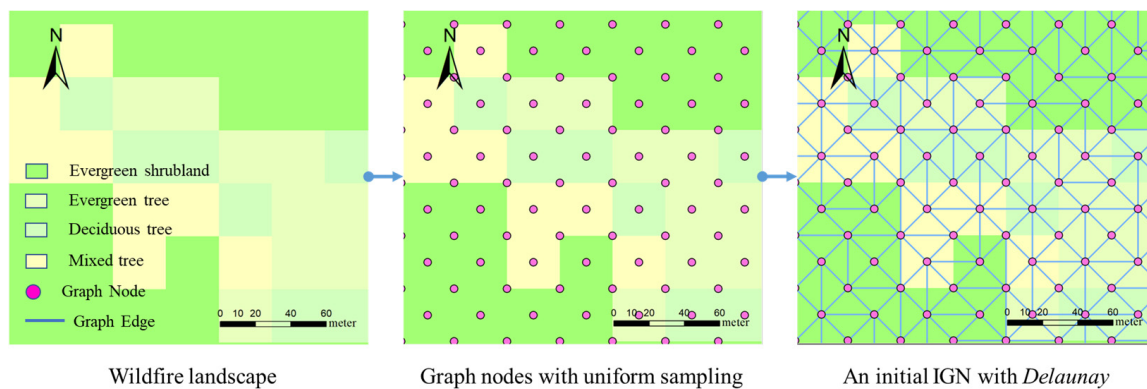


Figure 2. IGN initialization.

2.2.3. IGN Adaptive Optimization

Adaptive optimization aims to dynamically adjust the node distribution of the IGN to eliminate edge heterogeneity. An IGN with GR_{min} might well characterize a regional landscape with single vegetation and a gentle slope, but it fails to maintain the homogeneity of the graph edges when the landscape is complex, in which case graph nodes are adaptively added to eliminate the heterogeneity of graph edges, as illustrated in Figure 3a. Therefore, an adaptive optimization method with three steps is implemented, as shown in Figure 3b. The first step is edge interpolation, where the edge is pre-interpolated with GR_{max} to form a candidate node set $Edge^i = \{n_0^i, n_1^i, \dots, n_M^i\}$, n_0^i and n_M^i are the start and target nodes of the i th edge, respectively. $M + 1$ is the total number of nodes in the interpolated edge. Each node has an independent temporary property A_m^i . The second step is a homogeneity check. When the fuel type of node n_m^i is different from that of the previous neighboring node n_{m-1}^i , it means that there is fuel heterogeneity in the edge, and node n_m^i is formally inserted into the graph nodes. ED_m^i is the elevation difference between nodes n_m^i and n_{m-1}^i , and similarly, ED_{m-1}^i is the elevation difference between nodes n_{m-1}^i and n_{m-2}^i . If the absolute difference between ED_m^i and ED_{m-1}^i exceeds a threshold T_{ed} , it means that an unacceptable slope change exists at node n_m^i . To ensure the slope homogeneity, node n_m^i is inserted into the graph nodes. The details of the adaptive process can be found in the pseudo-code in Appendix B. Third, the properties of the newly inserted nodes are generated, and an updated IGN is reconstructed by the Delaunay algorithm. The above steps iterate until no new nodes are inserted, then the graph nodes whose connected nodes are all non-combustible are taken as redundant nodes and removed. The spatial distribution of graph nodes is determined, and the final variable-scale IGN is constructed.

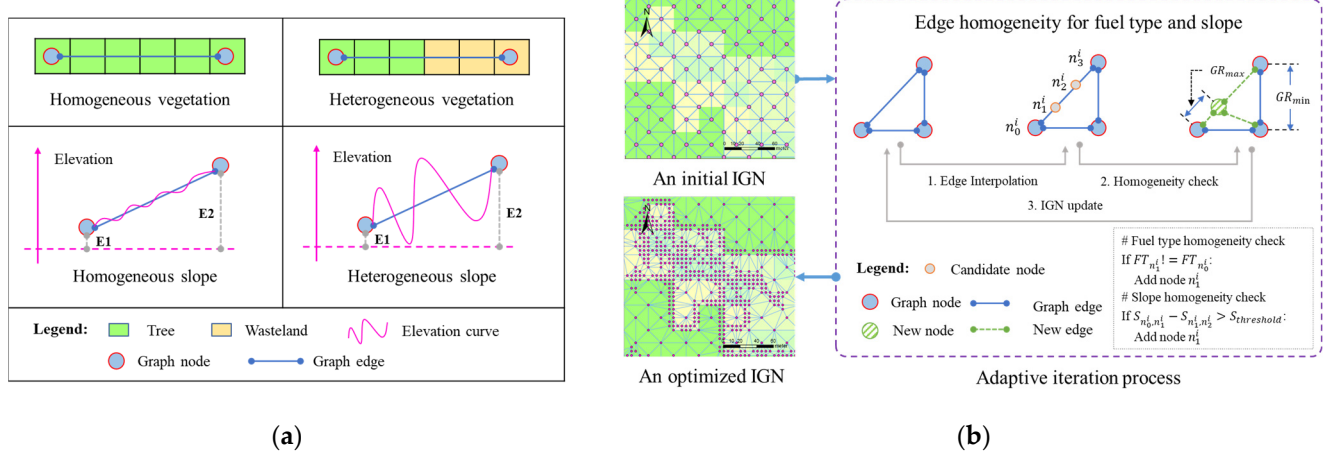


Figure 3. IGN adaptive optimization. (a) Homogeneity and heterogeneity in fuel and slope; (b) adaptive iteration process for IGN optimization.

As stated in the adaptive optimization process, T_{ed} is an important factor that determines the structure of IGN. As when T_{ed} is smaller, the homogeneity check in IGN optimization will be more sensitive to slope changes. It indicates that more graph nodes will be inserted, and the graph refinement will be higher, and vice versa. Therefore, it is necessary to analyze the effect of different T_{ed} values on the IGN structure, and then select the optimal value, as we discussed in Section 4.2.

2.3. Deep Learning-Based Spread Model

2.3.1. Definition of the IGN Spread

The spread of wildfire in the IGN is different from the grid-based model. The existing graph-based model adopted the elliptical fire model to calculate the rate of spread in the IGN. However, the computational solution is fairly complex when the wind direction

and edge angle are different. Therefore, we design a deep learning-based spread model named *WFDNN* (wildfire deep neural network) to simplify the calculation process. We first introduce VSEs (valid spread edges) and VSNs (valid spread nodes) to illustrate the spread process in the IGN-based landscape. The ignition time T^i of graph node n^i is determined by its connected ignited nodes. Suppose the set of graph nodes connected with node n^i is $N^i = \{n_0^i, n_1^i, \dots, n_M^i\}$, the ignition time of N^i is $T_{con}^i = \{T_0, T_1, \dots, T_M\}$, the spread time from N^i to node n^i is $t_{con}^i = \{t_0, t_1, \dots, t_M\}$, and $M + 1$ is the number of connected nodes. Here, we sum over T_{con}^i and t_{con}^i as the candidate ignition time of node n^i , then choose the minimum time as the T^i . The ignited node corresponding to the minimum time is taken as the VSN of node n^i , and the edge formed by node n^i and the VSN is defined as the VSE. Therefore, the wildfire simulation in the IGN landscape is composed of these VSNs and VSEs, which explicitly points out the spread route from the ignition to these unburned areas.

2.3.2. Construction of Grid-Based Dataset

After defining the VSN and VSE, a training dataset is constructed to provide samples to train the *WFDNN* model. First, we select the FARSITE model [36] as the simulator to generate ground truth labels. Here, real wildfire cases are not used to construct the dataset. This is because publicly available comprehensive case data records are few. Therefore, these limited cases fail to meet the data requirements of *WFDNN*. In contrast, the input data of the FARSITE model are relatively easy to obtain from USGS data [73]. This mature model has been widely used for wildfire experiments [76,81–83]. Other models are also available to generate datasets, such as *BehavePlus* [33], *WRF-SFIRE* [84] and *WFA* [85]. Then, we download essential landscape (lcp) data from USGS LANDFIRE [86] and up-sample the spatial resolution to GR_{max} (5 m). The lcp file is a special multi-band raster format for FARSITE model and consists of eight bands (fuel model, elevation, slope, aspect, canopy cover, canopy base height, canopy bulk density, and stand height) [87]. Next, we clip the lcp data into small patches with the size 500 m \times 500 m, and 70 patches are generated with the filter criterion that a patch should contain more than 85% vegetation coverage. Here, the vegetation coverage is determined by the fuel model layer from the lcp file. For each patch, 10 stochastic wildfires that burned for 1 h are simulated by the FARSITE model, where weather data are random values generated by a uniform distribution (weather data contain wind speed, wind direction, temperature, humidity, and their threshold ranges are 0–12 m/s, 0–2 π , 10–25 °C, and 5–20%, respectively), and fire ignitions are random points within the central neighborhood of the patch region. As the position of a fire ignition may not fall exactly on a graph node, we choose the nearest graph node to the ignition as the ignition node and set the ignition time property of the ignition node to 0. Finally, seven hundred simulated wildfires are generated, but these simulations are grid-based results.

2.3.3. Construction of IGN Dataset

To convert these grid-based simulations into graph-based simulations, a Grid-Graph matching method is implemented for the graph landscape, as Figure 4 shown. Based on the same coordinate system, the IGN is overlaid with the grid-based simulations. Then, we map the ignition time property of the grid to the graph node at the corresponding position. Thus, the graph node becomes equipped with the ignition time label. Next, an empirical VSE extraction method is adopted to determine the VSNs and VSEs in these labeled graph nodes. Suppose that node n^i is a labeled graph node with ignition time T^i , its connected nodes is $N^i = \{n_0^i, n_1^i, \dots, n_M^i\}$, the ignition time of N^i is $T_{con}^i = \{T_0, T_1, \dots, T_M\}$, and $M + 1$ is the number of connected nodes. Thus, the spread time from N^i to node n^i can be calculated as $t_{con}^i = \{T^i - T_0, T^i - T_1, \dots, T^i - T_M\}$. If t_m^i is greater than 0, it means that node n^i is ignited after the connected node n_m^i , and vice versa. Then, we remove these nodes with $t_m^i < 0$ as they are ignited later and impossible to ignite the node n^i . When dealing with the complex landscape, it is difficult to infer the VSN based on ignition time alone since the VSN is determined by both ignition time and spread time, as discussed in Section 4.3. Thus,

the empirical formulas $ts = f_{emp}(\theta)$ in the grid-based model [27] is adopted to calculate the spread time ts_{con}^i of graph edges N^i . Due to the differences in landscape representations, it is natural that there is an offset between t_{con}^i and ts_{con}^i . We think this offset of the VSE is the minimum relative to other connected edges. The details of the Grid-Graph matching algorithm can be found in the pseudo-code in Appendix C. Take the demo in Figure 4 as an example, the offset in ts_2^i and t_2^i ($t_2^i = T - T_2$) is the minimum, the node n_2^i is taken as the VSN of node n^i , the edge formed by node n^i and the VSN n_2^i is defined as the VSE. We notice that T_1 is similar to T , as node n_1^i and node n^i are almost ignited by the node n_2^i at almost the same moment. Here, node n_1^i is not taken as the VSN, as the spread time t_1^i from node n_1^i to node n^i is much greater than t_1^i ($t_1^i = T - T_1$) while the wind direction is 45° . Finally, based on the empirical method, total 65,505 VSEs are extracted from the 700 grid-based labels. To train the WFDNN, we adopt a 4:1 ratio to divide the VSEs in the IGN dataset into 52,404 training VSEs and 13,101 test VSEs, respectively.

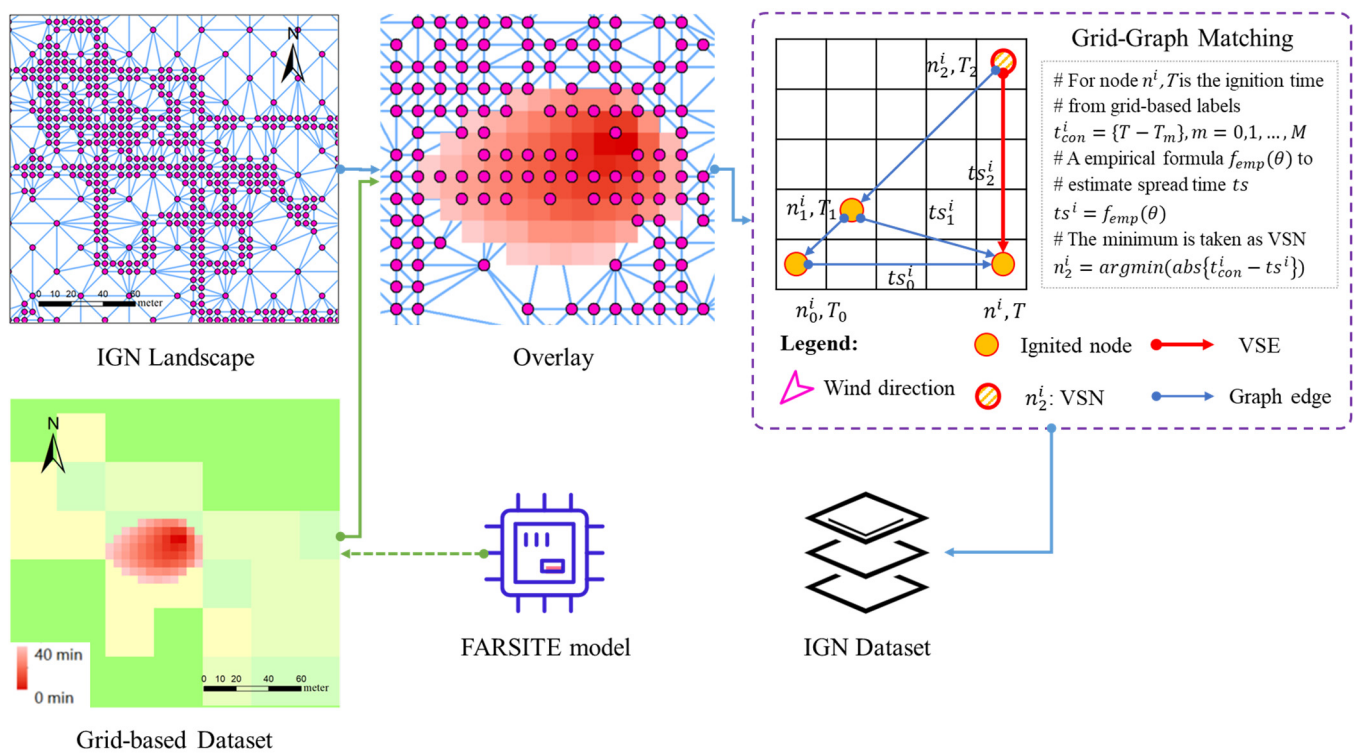


Figure 4. Construction process of IGN dataset with Grid-Graph matching method.

2.3.4. Design of Deep Neural Network

To rapidly and accurately calculate the spread time of each graph edge, we design the deep neural network WFDNN to fit a nonlinear formula \hat{f} and predict the spread parameters from the ignited node to the unignited node,

$$\mathcal{L}(\hat{t}, \hat{f}l, \hat{f}i; t, fl, fi) = \hat{f}(Fuel, Length, Slope, Angle, WD, WS, TE, H), \tag{6}$$

where *Fuel*, *Length*, *Slope*, and *Angle* are fuel type, edge length, slope, and azimuth angle, respectively. *WD*, *WS*, *TE*, and *H* are wind direction, wind speed, temperature, and humidity, respectively. *t*, *fl*, *fi* is the ground truth of the spread time \hat{t} , the flame length $\hat{f}l$, the fire intensity $\hat{f}i$. \mathcal{L} is an L1 loss function used to calculate the difference between the prediction \hat{y} and the ground truth *y*. Take the spread time as an example; the L1 loss is defined as $\mathcal{L} = |\hat{t} - t|$. The architecture of the WFDNN is shown in Figure 5.

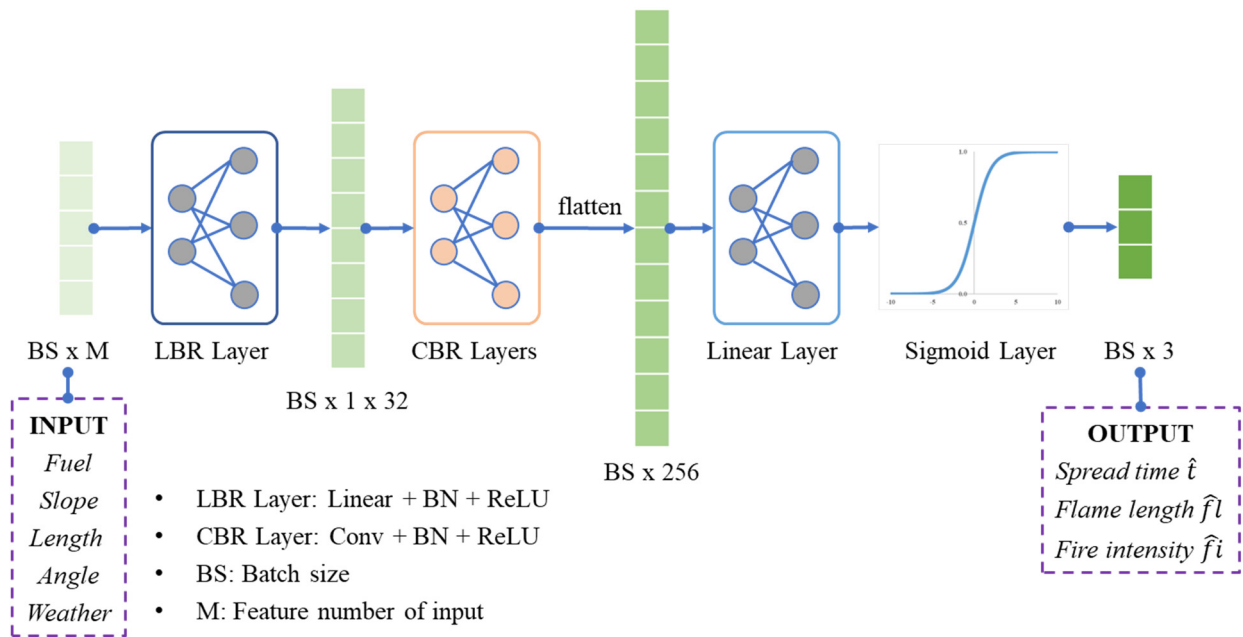


Figure 5. Network architecture of WFDNN.

WFDNN consists of two hybrid layers, a linear layer and an activation layer. The first hybrid layer is an LBR (Linear + BN + ReLU) layer, composed of a linear layer (Linear), a batch normalization (BN) layer, and a linear rectification (ReLU) layer. The linear layer is a linear transformation defined in Equation (7),

$$v = xA^T + b, \tag{7}$$

where x and v are the input and output tensor, respectively. A^T is the transformation matrix, and b is the bias matrix. This linear operation is essentially matrix multiplication and addition, mapping the input x into a higher dimensional tensor v . The BN layer [88] is a normalization operation, transforming the input tensor into a normal distribution with mean $u = 0$ and variance $\sigma = 1$, as defined in Equation (8).

$$\omega = \frac{x - E[v]}{\sqrt{Var[v] + \epsilon}} * \gamma + \beta, \tag{8}$$

where $E[\cdot]$ and $Var[\cdot]$ are the expectation and variance of the input tensor v , respectively. γ and β are learnable parameter vectors, and ϵ is a small value added to the denominator for numerical stability. This BN layer is able to prevent gradient explosion or disappearance and accelerate network convergence. By contrast, as one of the activation layers, the ReLU layer [89] is designed to incorporate the nonlinear function into the network and improve the network’s ability to fit the sample data, as defined in Equation (9).

$$y = ReLU(\omega) = (\omega)^+ = \max(0, \omega), \tag{9}$$

This hybrid layer maps the input tensors ($BS \times 1 \times M$) to a high-order tensor ($BS \times 1 \times 32$), where BS is the batch size and set as 32, and M is the feature number of the VSE and determined by Equation (6). The second hybrid layer contains five CBR (Conv + BN + ReLU) layers; each CBR layer is composed of a convolution (Conv) layer, a batch normalization (BN) layer, and a ReLU layer. The convolution layer [90] is implemented with local connectivity and weight sharing to extract features from the input tensor. As the number of convolutional layers increases, deeper features of the input tensor can be extracted. The first CBR layer is designed to generate the higher-order features ($BS \times 32 \times 32$), and the remaining four CBR layers are implemented with the same kernel

number and extract deeper features ($BS \times 64 \times 4$). The last linear layer and sigmoid layer are designed to regress a prediction tensor ($BS \times 3$), consisting of the spread time \hat{t} , the flame length $\hat{f}l$, the fire intensity $\hat{f}i$ of the input graph edges. The sigmoid layer [91] is another type of activation function and converts any input into a value between 0 to 1, as defined in Equation (10).

$$\sigma(x) = \frac{1}{1 + e^{-x}}, \quad (10)$$

When the *WFDNN* was trained on the IGN dataset with the back-propagating learning method, the minimum travel time algorithm was then adopted to iteratively calculate the ignition time of each graph node from the ignition node under dynamic weather conditions. The spread of wildfire can be explicitly demonstrated in a novel graph structure with crucial wildfire characteristics, such as spread rate, flame length, and fire intensity. To better analyze wildfire, the values of these characteristics can be classified into specific categories with custom thresholds. The number of categories and the range of values are flexible and can be dynamically adjusted according to the actual requirements.

3. Results

3.1. WFDNN Result

The deep neural network *WFDNN* is implemented by *PyTorch*; the initial learning rate is 0.001, the optimizer is Adam, and the loss function is L1 loss. After 100,000 iterations, the *WFDNN* converges with a loss value of 0.061, as shown in Figure 6a. On the test dataset, the trained *WFDNN* shows competitive performance compared with the FARSITE model and CA model. The inference time is 0.0017 s for each sample, and the mean absolute error is 0.936 min, 0.895 feet, and 177.2 kw/m on spread time, flame length, and fire intensity, respectively, as shown in Figure 6b.

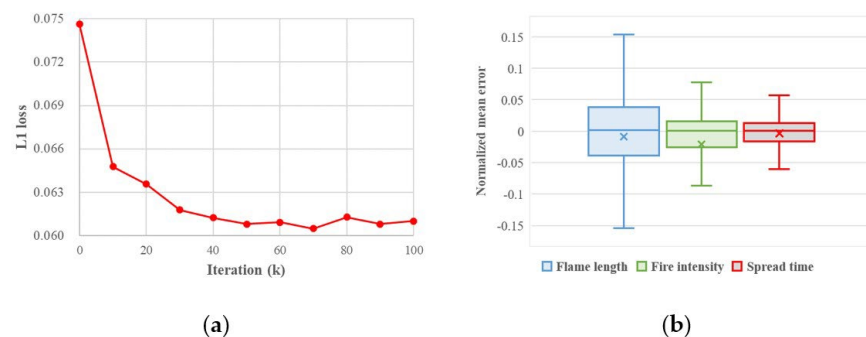


Figure 6. Performance of *WFDNN*. (a) Training curve; (b) test error.

3.2. Results of Getty Fire Case

As shown in Figure 7, the simulation results of the above three models are displayed and categorized by a 2-h time interval. In terms of model refinement, the simulations with the high-resolution landscape are more refined than those with low resolution. They naturally contain more details about the wildfire spread process. In contrast, the IGN model adopts a variable scale landscape and demonstrates the spread of wildfire with a spatiotemporal spread route. Figure 7e shows the local route of IGN simulation, which clearly describes the fire spread from the ignition to the surrounding unburned area. Obviously, a higher refinement of the model will lead to lower computational efficiency. The runtimes of the above five scenarios (Figure 7a–d) are 15.864 s (FARSITE-30 m), 45.809 s (FARSITE-5 m), 0.954 s (CA-30 m), 56.431 s (CA-5 m), and 82.888 s (IGN), respectively. The higher refinement notably improves the model computation time. We should note that the runtime of the FARSITE model is sensitive to the “Perimeter Resolution (PR)” parameter. In the high-resolution scenario, when the PR is set to 30 m, 20 m, and 10 m, the simulation runtime is 45.809 s, 1 min 59.076 s, and 9 min 45.809 s, respectively. When the PR is set to 5 m, the FARSITE model cannot output the results within the limited hourly waiting time.

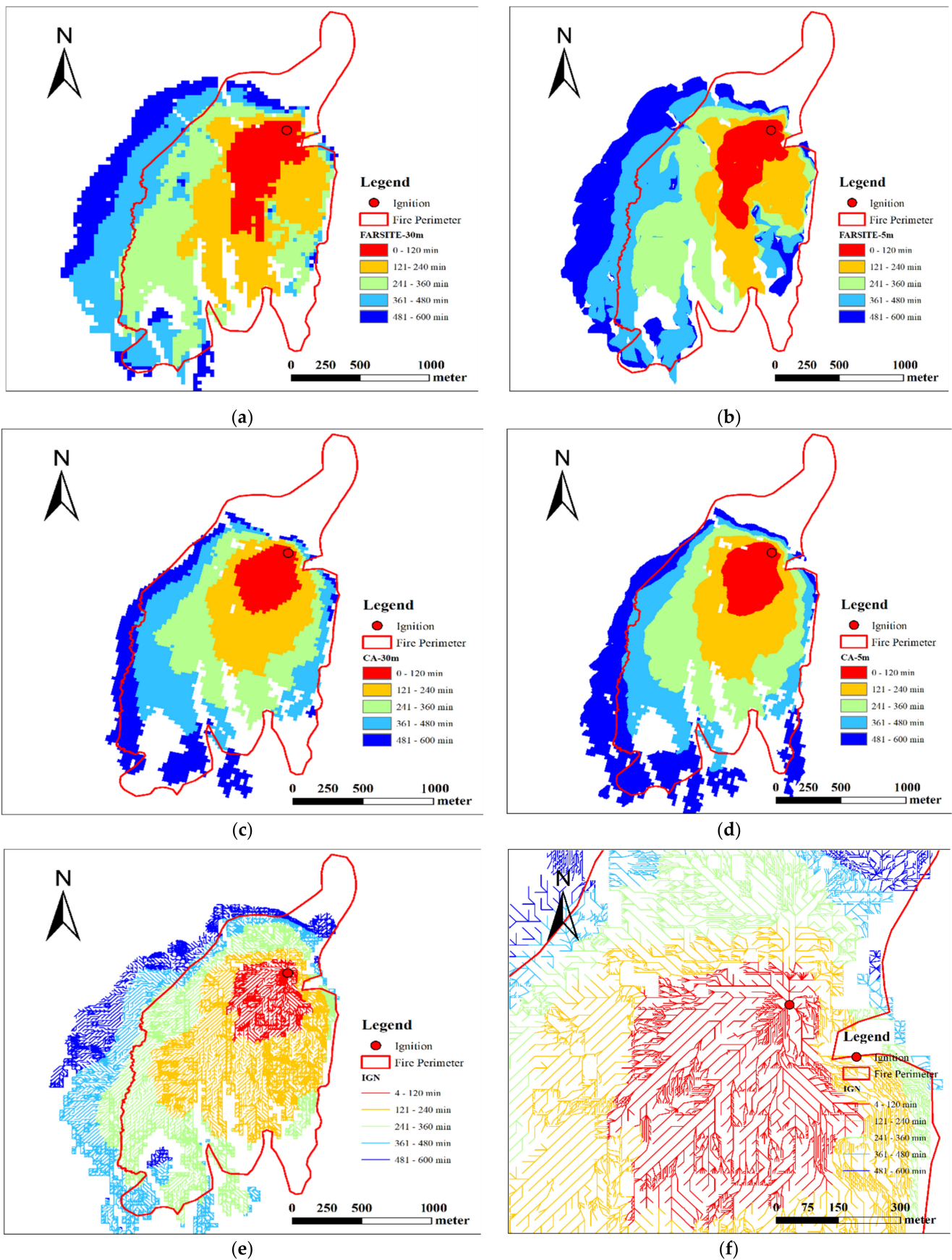


Figure 7. Experimental simulation results. (a) FARSITE model [30 m]; (b) FARSITE model [5 m]; (c) CA model [30 m]; (d) CA model [5 m]; (e) IGN model; (f) local IGN results.

The burned area comparison of the above three models is presented in Figure 8a. The area of the record data (red line) increases steadily from 0 to 150 min, then grows rapidly from 150 to 200 min, and next turns slow until the wildfire is gradually under containment by firefighters. The IGN model (pink line) maintains the best performance with an average area error (AAE) of 109.43 and has the closest value with the record at any time (111 min: 33 acres, 171 min: 17 acres, 191 min: 153 acres, 216 min: 312 acres, 281 min: 169 acres, 406 min: 62 acres, and 446 min: 20 acres). At the same time, other models (FARSITE-5 m, FARSITE-30 m, CA-5 m, and CA-30 m) perform with AAE 277.43 acres, 171 acres, 257.29 acres, and 279.71 acres, respectively. The model performances with Jaccard, SM, and OA are illustrated in Figure 8b; three models all demonstrate competitive performance in the Getty Fire case. CA model has the best performance (Jaccard: 0.624, SM: 0.769, OA: 0.843). Although the performance of the IGN model (Jaccard: 0.587, SM: 0.740, OA: 0.800) is slightly lower than the CA model, it has an advantage over its baseline model, FARSITE model (Jaccard: 0.564, SM: 0.721, OA: 0.801).

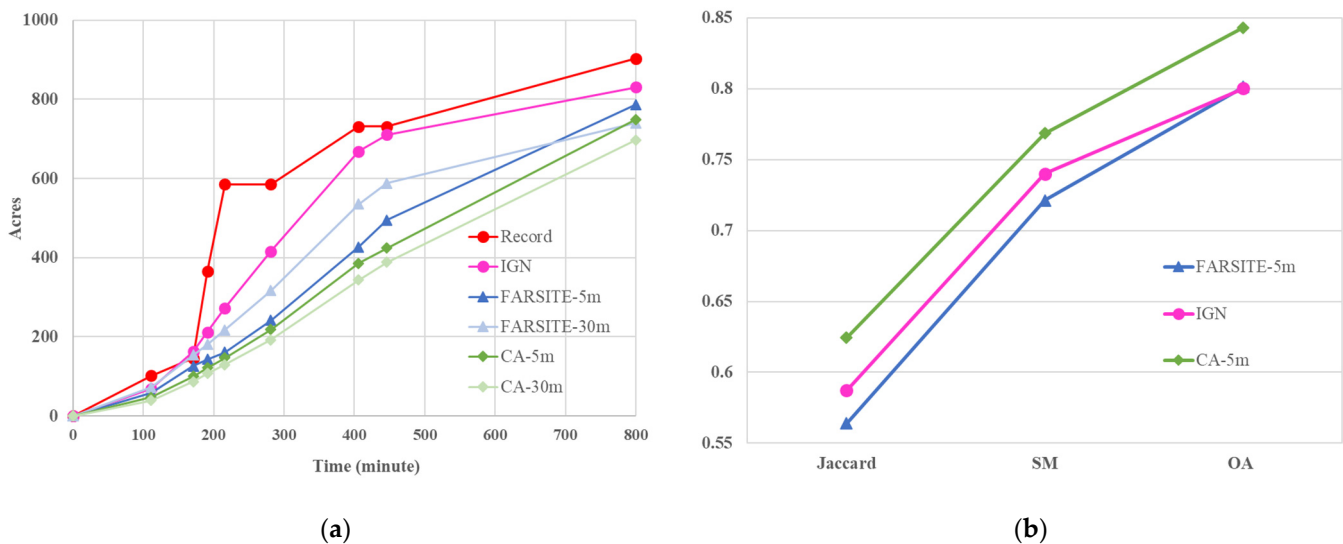


Figure 8. Quantitative comparative analysis. (a) Comparison of the burned area at different times; (b) comparison of model performance.

In addition to the wildfire spread route, the IGN model is also able to demonstrate other crucial wildfire characteristics in the graph form, such as spread rate, flame length, and fire intensity, as shown in Figure 9. Here, the spread rate is divided into 0–20 km/h (Green), 21–50 km/h (Blue), and >50 km/h (Red), while the flame length and fire intensity are divided into 0–1 feet (Green), 2–3 feet (Blue), >3 feet (Red), and 0–150 kw/m (Green), 151–300 kw/m (Blue), >300 kw/m (Red), respectively.

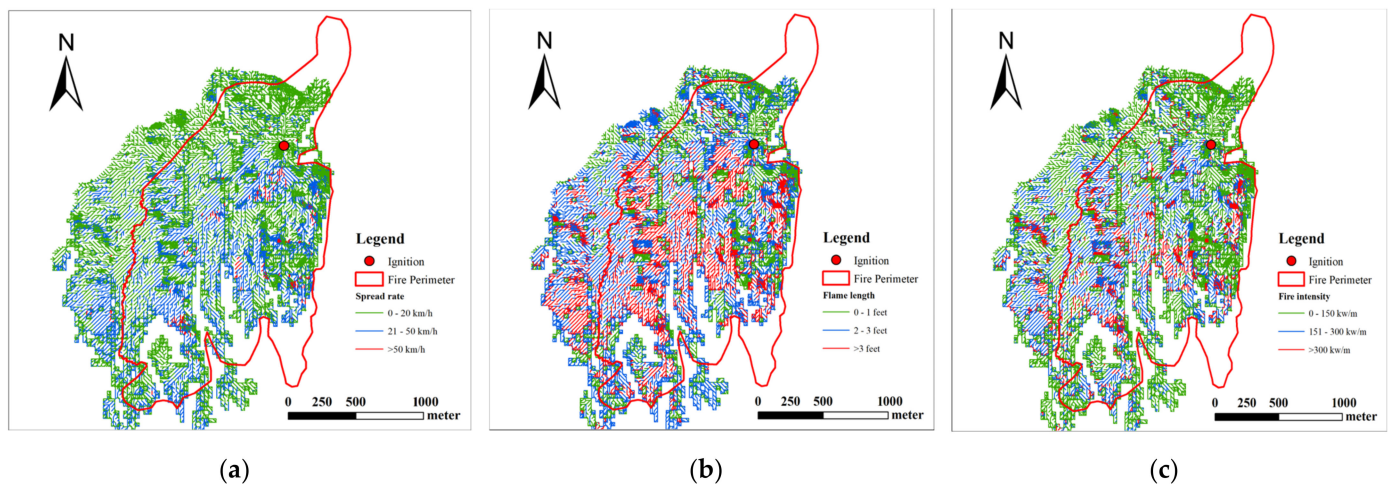


Figure 9. Wildfire spread characteristics in IGN-based landscape. (a) Spread rate; (b) flame length; (c) fire intensity.

4. Discussion

4.1. Analysis of Getty Case

As for the computational efficiency, the CA model has a significant computational advantage in the low-resolution scenario compared to FARSITE and IGN models, whereas CA model only calculates the ignition time of raster grids and does not involve the prediction of spread rate, flame length, and fire intensity. IGN model has the same order of magnitude of computation time as the other models and is about 30 s slower than the FARSITE and CA models with 5-m resolution. This is mainly due to the fact that the computer is more suitable for the calculation of raster grids instead of the graph structure. This difference in model runtime can be reduced when multiprocessor computing systems such as computational clusters based on Message Passing Interface (MPI) paradigm are adopted.

The final wildfire perimeter recorded by GeoMAC [74] was adopted to evaluate model performance. The perimeter area is about 704 acres, while the record in LAFD [72] is near 800 acres at 600 min. This is mainly due to measurement errors and the difference in calculation methods of different government agencies. Additionally, it should be noted that the recorded area contains some measurement errors (the recorded area at 216 min and 281 min is the same, and at 406 and 446 min as well), as it is difficult to accurately obtain the area from the remote sensing imagery or GPS tracker, especially when the wildfire is still burning and spreading.

In addition, we found that the IGN model slightly outperformed the FARSITE model. Nevertheless, it seems more reasonable that the FARSITE model performs better than the IGN model, as the training datasets for the IGN model are all from the baseline FARSITE model. This might be explained as there are measurement errors in the recorded fire perimeter and data deviation in model input. For example, the dynamic weather data are downloaded from a nearby weather station, and they are not able to accurately describe the wind field in the wildfire region. Therefore, the evaluation metrics for the simulation and the real record contain some errors, which might lead to the result that the IGN model slightly outperformed the baseline model in this fire case.

The wildfire spread characteristics are crucial to avoid firefighter entrapments [8]. When the value of spread rate, flame length, or fire line intensity is too large, there would be a higher likelihood of triggering entrapment and causing firefighter injury or even death. Therefore, firefighters should avoid these high-risk areas or take measures in advance to block the spread of wildfires, such as firebreaks. Furthermore, the graph-based wildfire simulation model is enlightening for other wildfire research, such as safety zones [92] and escape routes [93].

4.2. Effect of Elevation Difference Threshold on IGN

Here, we discuss and compare the graph network characteristics under three thresholds ($T_{ed} = 1$ m, 3 m, and 5 m). A patch with size 500 m \times 500 m was selected as the case and processed by our IGN generation algorithm. The numbers of graph nodes and edges are 9538 ($T_{ed} = 1$ m), 6089 ($T_{ed} = 3$ m), 2101 ($T_{ed} = 5$ m), and 28,300 ($T_{ed} = 1$ m), 18,131 ($T_{ed} = 3$ m), 6218 ($T_{ed} = 5$ m), respectively. Figure 10 shows the local graph structures of different thresholds T_{ed} . To better describe the IGN characteristics, we define the graph edges with lengths less than 10 m as short edges while others as long edges. when T_{ed} is 1 m, the IGN structure is the most complex, and 99% of graph edges are short edges. This IGN contains rich landscape, but its data volume is too large and the redundancy is high. While T_{ed} is 3 m, the IGN structure is simplified but still dominated by short edges, accounting for 88% of the total number of graph edges. When further increasing the threshold T_{ed} to 5 m, the percentage of short edges drops to 58%, enabling to balance the model refinement and data redundancy. Therefore, T_{ed} is set as 5 m in our IGN optimization part, and the IGN model with this threshold shows prominent performance and is verified on the real wildfire Getty Fire case.

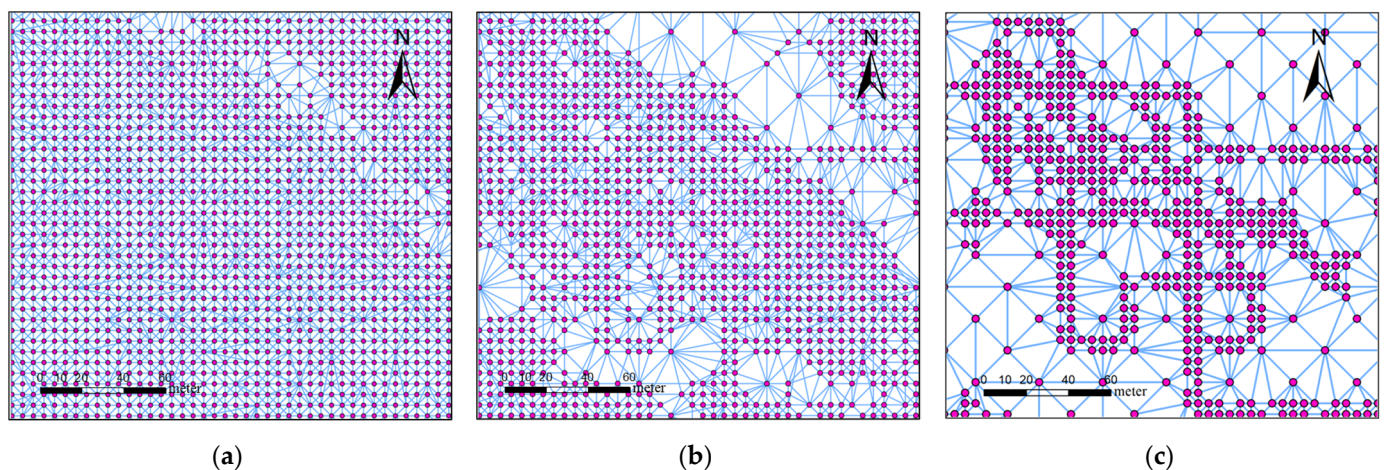


Figure 10. IGN structure with different T_{ed} . (a) $T_{ed} = 1$ m; (b) $T_{ed} = 3$ m; (c) $T_{ed} = 5$ m.

4.3. VSE Dataset Analysis

VSN and VSE are defined to describe the graph node that first ignites another node and the graph edge they form. However, it is not an easy task to determine the VSN and VSE when generating the IGN dataset from the grid-based dataset, as we only know the ignition time of the graph node and cannot accurately infer the VSN from the connected nodes. Therefore, we have proposed several methods to generate the IGN dataset, such as the empirical method (EMP), the maximum time method (MAX), and the all-extraction method (ALL). The empirical method is illustrated in Section 2.3.2, while the maximum time method thinks that the larger the ignition time difference between the nodes, the larger contribution of the ignition effect. Thus, this method considers the edge with the maximum spread time among all connected graph edges as the VSE. In contrast, the all-extraction method takes all graph edges with a spread time greater than zero as VSEs, as all connected edges are contributors to the ignition of the target node. Based on the above three methods, the number of generated VSEs in the IGN dataset is 65,505 (EMP), 80,821 (MAX), and 210,116 (ALL), respectively. Each dataset is randomly divided into training and testing sets according to the ratio of 4:1 and further adopted to train and test WFDNN. As Figure 11a,b shows, the empirical method converges faster and has the smallest loss value (EMP loss: 0.061, MAX loss: 0.086, ALL loss: 0.091). In addition, the empirical method maintains the advantage in test error of spread time (EMP loss: 0.936 min, MAX loss: 1.999 min, ALL loss: 2.147 min), flame length (EMP loss: 0.895 feet, MAX loss: 0.721 feet, ALL loss: 0.962 feet) and fire intensity (EMP loss: 177.2 kw/m, MAX loss: 180.0 kw/m, ALL loss: 179.1 kw/m).

Moreover, the Getty Fire case was taken to compare the above three methods from a visual perspective, as shown in Figure 11c–e. Although there is only a slight difference in the values of the model training and testing, it is evident in the case that the simulation results of these methods have notable differences. These results show that *WFDNN* trained by the empirical method is able to simulate the wildfire and generate predictions that fit well with the recorded fire perimeter. However, the *WFDNN* performs poorly with the datasets constructed by the other two methods (MAX and ALL). The prediction results are significantly different from the real recorded perimeter, which indicates maximum time method and all-extraction method are inappropriate for application in actual wildfire spread prediction.

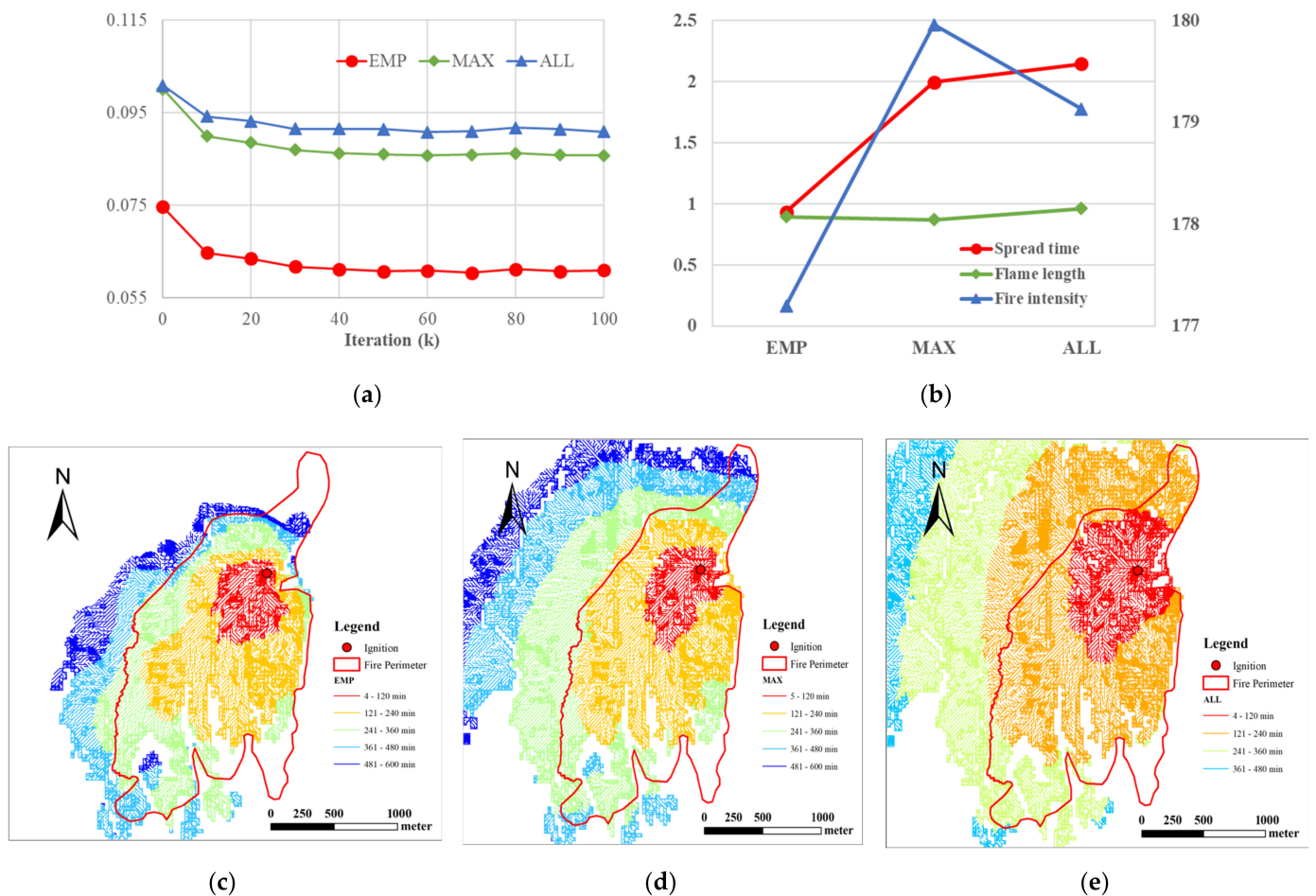


Figure 11. Comparison of different VSE dataset construction. (a) Training curve; (b) test error; (c) empirical method; (d) maximum time method; (e) all-extraction method.

5. Conclusions

A wildfire spread model can provide explicit guidance for emergency rescue. Most such models use regular grids or perimeter polygons to represent the wildfire landscapes. These grid-based models divide the spatial landscape into adjacent regular cells and calculate the moment when a cell is ignited, while the polygon-based models adopt the Huygens principle and predict the fire perimeters at given moments. However, it is difficult for the above models to explicitly demonstrate the spatiotemporal details of wildfire spread, such as the spread route, especially in complex landscapes.

We proposed a wildfire spread model with an irregular graph network (IGN). An IGN generation algorithm was implemented to characterize the wildfire landscape with a variable scale, enabling to adaptively optimize the graph node density and graph edge connection according to the region complexity. This irregular representation solves the

problem of choosing the best resolution in the grid-based landscape and realizes a novel mode to simulate the spread of wildfire. In addition, a deep learning-based spread model named *WFDNN* was designed for the special IGN landscape, which fit a nonlinear formula to predict the spread time, flame length, and fire intensity of graph edges under various environmental conditions. A real wildfire in Getty, California, US, was selected to demonstrate and evaluate our IGN model. Comparative experiments with the widely used FARSITE model and CA model showed that our model has the ability to simulate wildfire spread with competitive accuracy while maintaining competitive simulation refinement and computational efficiency. The IGN model is superior in describing the spatiotemporal characteristics of wildfires with an explicit spread route. This special graph route is equipped with crucial wildfire behavior properties such as ignition time, spread rate, flame length, and fire intensity, which are essential for emergency management agencies to make rescue plans and avoid entering potentially high-risk areas.

The present IGN is enlightening in wildfire spread prediction; however, there are still some limitations, and more future work is needed. First, the IGN model is a mathematical analog model that combines a graph network and deep neural network to model the spread of wildfires. It ignores physical and chemical processes such as inert heating, drying, pyrolysis, flame combustion, and coke afterburning accompanied by media movement and plume formation [21,22]. It would be worthwhile to directly incorporate the physical mechanism into the IGN model and further improve model performance. Second, this model does not incorporate the graph topology and ignores the thermal effect of these non-VSNs. The prediction error tends to be magnified when the spread times of connected graph edges are more similar, as other graph nodes play as important a role as the VSN node. Therefore, it would be interesting to adopt the graph convolutional network (GCN) [63] to model the graph topology and predict the wildfire spread in the graph mode, but the computation method in this GCN model would be complex and hard to design, as the number of connected nodes is variable and computational resources are limited.

Author Contributions: Conceptualization, F.W., W.J. and G.S.; methodology, W.J., F.W. and X.L.; software, W.J. and G.W.; formal analysis, Q.M.; data curation, X.L., X.Z. and T.W.; writing—original draft preparation, W.J.; writing—review and editing, F.W. and G.S.; visualization, W.J. and Q.M.; supervision, F.W. and G.S.; funding acquisition, F.W. All authors have read and agreed to the published version of the manuscript.

Funding: This research was funded by the Disciplines Distribution Project of Shenzhen, China (Grant Number: JCYJ20180508152055235) and the Key Field Research and Development Program of Guangdong, China (Grant Number: 2019B111104001).

Data Availability Statement: Requests for more data can be addressed to the corresponding author.

Conflicts of Interest: The authors declare no conflict of interest.

Appendix A

The differences between three models (FARSITE, CA, and IGN) are summarized and explained in Table A1.

Table A1. Model comparison.

	FARSITE	CA	IGN
Theoretical principle	Thermal physics	Thermal physics	Deep learning
Spread pattern	Huygens	Cellular automata	Graph network
Landscape type	Vector	Grid	Vector
Output format	Polygon or Grid	Grid	Graph

(1) Theoretical principle

The kernel principles of FARSITE and CA models are the same, as they both rely on thermal physics theory and ignition experiments to construct mathematical equations. In

contrast, the IGN model proposes a deep neural network named *WFDNN* to construct these complex equations. The sample dataset to train the *WFDNN* is generated by FARSITE model (surely other suitable models can also be alternative). Thus, the *WFDNN* indirectly inherits some thermophysical properties.

(2) Spread pattern

After implementing the mathematical equations, a spreading model is needed to realize the extrapolation from a fire ignition to the unburned area. There are significant differences in the spread patterns of the three models. Based on the Huygens principle, the FARSITE model defines the wildfire landscape as a continuous space and adopts an elliptical model to calculate the spread range of the next moment at the sampling point of the wildfire boundary, while the CA model is designed based on the principle of cellular automata, which divides the wildfire landscape into adjacent regular grids and calculates the cumulative influence of the central cell pair on the neighboring cells. In contrast, our IGN model innovatively takes an adaptive irregular graph network to characterize the wildfire landscape and calculates the spread of wildfires from the graph nodes along the graph edges.

(3) Landscape type

FARSITE and IGN are vector landscapes, while the CA model is the grid landscape. The landscape type is mainly determined by the spread pattern that the model adopts.

(4) Output format

The FARSITE model is able to output the simulation results in both polygon (fire perimeter) and grid format, while the CA model only outputs the grid format. In comparison, our IGN model defines the simulation in a novel graph network format, enabling it to explicitly describe the spread details of wildfire.

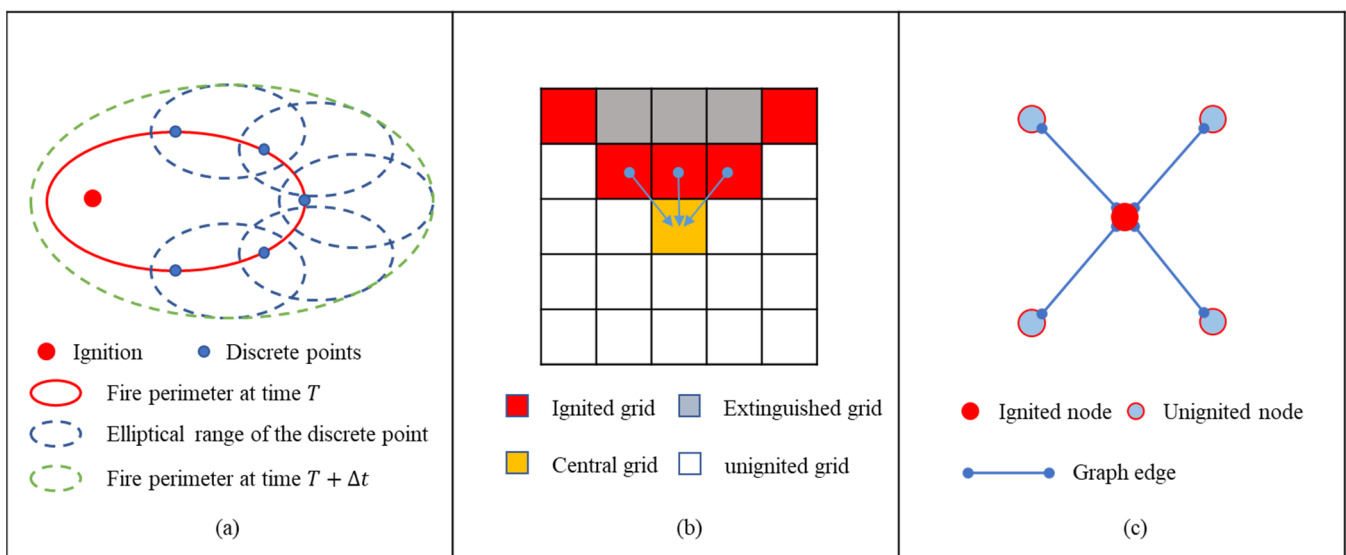


Figure A1. Spread patterns. (a) FARSITE model; (b) CA model; (c) IGN model.

Appendix B

The adaptive iteration process is crucial for graph edge homogeneity. To explain it more clearly, we use pseudo-code to elaborate on the details, as Algorithm A1 shows.

Algorithm A1 Adaptive iteration process in IGN optimization.

```

# INPUT :  $G_{int}$ , the initial IGN with uniform sampling and Delaunay algorithm
# OUTPUT :  $G_{opt}$ , the optimized IGN
 $(V, E) = G_{int}$  is the edges of the graph network
 $V_{new} = \text{null}$  # To store newly inserted nodes
Iter_counter = 0 # Count the time of iteration
Iter_count_max = 1e3 # The maximum time of iteration
# Adaptive iteration
while True:
    # count the number of iteration
    Iter_counter += 1
    for each  $edge^i \in E$ :
        # Step 1: Edge interpolation. Use equally spaced interpolation to obtain a candidate
        node set
         $\{n_0^i, n_1^i, \dots, n_M^i\} = \text{Interpolate}(edge^i)$ 
         $NC^i = \{n_0^i, n_1^i, \dots, n_M^i\}$  # Candidate node set, containing M+1 nodes
        # Step 2: homogeneity check: fuel type and slope
        for each  $n_m^i \in NC^i$ : # fuel type
            if  $FT_{n_m^i} \neq FT_{n_{m-1}^i}$ :
                # The fuel type changes in the  $edge^i$ , thus we add the node to avoid the
                heterogeneity.
                 $V_{new}.add(n_m^i)$  # add node  $n_m^i$  into  $V_{new}$ 
        # Slope homogeneity. Here we use elevation difference to replace
         $ED_{NC^i} = \text{Get\_ED}(NC^i)$  # Get elevation differences of neighboring nodes
        for each  $ED_m \in ED_{NC^i}$ :
            if  $ED_m - ED_{m-1} > T_{ed}$ :
                # The elevation has a large wave, thus we add the node to eliminate it.
                 $V_{new}.add(n_m^i)$  # add node  $n_m^i$  into  $V_{new}$ 
        # Step 3: Reconstruct the IGN by Delaunay algorithm,
         $V_c = \text{Concatenate}(V, V_{new})$  # Concatenate and generate new node set
         $G = \text{Delaunay}(V_c)$  # Update the G with new nodes
         $(V, E) = G$ 
        # if no more new nodes or reaching the maximum iteration
        If  $\text{is\_null}(V_{new})$  or  $\text{Iter\_counter} > \text{Iter\_count\_max}$ :
            Break
# Get the  $G_{opt}$ 
 $G_{opt} = G$ 

Return  $G_{opt}$ 

```

Appendix C

The Grid-Graph matching algorithm is crucial to generate the IGN dataset. To explain it more clearly, we use pseudo-code to elaborate on the details, as Algorithm A2 shows.

Algorithm A2 Grid-Graph matching algorithm.

```

# graph network;  $L_{grid}$  grid-based labels
# OUTPUT :  $L_{graph}$ , graph-based labels
# and  $L_{grid}$ 
 $G_T = \text{Overlay}(G, L_{grid})$ 
# from the time in  $L_{grid}$ 
 $\{T_0, T_1, \dots, T_K\} = G_T$  is the number of graph nodes
# Set
VSEs = null
 $L_{graph} = \text{null}$ 
# Search the VSE and VSN
For each  $n^i \in G$ :
  # Get the spread time of each connected edge
   $T_{con}^i = \{T^i - T_m^i\}$ ,  $m = 0, 1, \dots, M$ . # M is the number of nodes connected with  $n^i$ 
  # Estimate spread time with an empirical formula  $f_{emp}$ 
   $ts^i = f_{emp}(\theta)$  is the proprieties of graph edges
# The minimum is taken as the VSE
   $j = \text{argmin}(\text{abs}\{T_{con}^i - ts^i\})$  # j is the index of the node with the minimum difference
  # Add the VSE
   $\text{VSEs.add}(\text{pair}\{n^i, n^j\})$ 
# Get the dataset
 $L_{graph} = \text{VSEs}$ 

Return  $L_{graph}$ 

```

References

- Bowman, D.M.J.S.; Balch, J.K.; Artaxo, P.; Bond, W.J.; Carlson, J.M.; Cochrane, M.A.; D'Antonio, C.M.; DeFries, R.S.; Doyle, J.C.; Harrison, S.P.; et al. Fire in the Earth System. *Science* **2009**, *324*, 481–484. [[CrossRef](#)] [[PubMed](#)]
- Doerr, S.H.; Santín, C. Global trends in wildfire and its impacts: Perceptions versus realities in a changing world. *Philos. Trans. R. Soc. B Biol. Sci.* **2016**, *371*, 20150345. [[CrossRef](#)] [[PubMed](#)]
- Godfree, R.C.; Knerr, N.; Encinas-Viso, F.; Albrecht, D.; Bush, D.; Cargill, D.C.; Clements, M.; Gueidan, C.; Guja, L.K.; Harwood, T.; et al. Implications of the 2019–2020 megafires for the biogeography and conservation of Australian vegetation. *Nat. Commun.* **2021**, *12*, 1023. [[CrossRef](#)] [[PubMed](#)]
- Ball, G.; Regier, P.; González-Pinzón, R.; Reale, J.; Van Horn, D. Wildfires increasingly impact western US fluvial networks. *Nat. Commun.* **2021**, *12*, 2484. [[CrossRef](#)] [[PubMed](#)]
- Zou, Y.; Rasch, P.J.; Wang, H.; Xie, Z.; Zhang, R. Increasing large wildfires over the western United States linked to diminishing sea ice in the Arctic. *Nat. Commun.* **2021**, *12*, 6048. [[CrossRef](#)]
- Tang, W.; Llort, J.; Weis, J.; Perron, M.M.G.; Basart, S.; Li, Z.; Sathyendranath, S.; Jackson, T.; Rodriguez, E.S.; Proemse, B.C.; et al. Widespread phytoplankton blooms triggered by 2019–2020 Australian wildfires. *Nature* **2021**, *597*, 370–375. [[CrossRef](#)]
- Minas, J.P.; Hearne, J.W.; Handmer, J.W. A review of operations research methods applicable to wildfire management. *Int. J. Wildland Fire* **2012**, *21*, 189–196. [[CrossRef](#)]
- Page, W.G.; Freeborn, P.H.; Butler, B.W.; Jolly, W.M. A review of US wildland firefighter entrapments: Trends, important environmental factors and research needs. *Int. J. Wildland Fire* **2019**, *28*, 551–569. [[CrossRef](#)]
- Sullivan, A.L. Wildland surface fire spread modelling, 1990–2007. 2: Empirical and quasi-empirical models. *Int. J. Wildland Fire* **2009**, *18*, 369–386. [[CrossRef](#)]
- Sullivan, A.L. Wildland surface fire spread modelling, 1990–2007. 1: Physical and quasi-physical models. *Int. J. Wildland Fire* **2009**, *18*, 349–368. [[CrossRef](#)]
- Sullivan, A.L. Wildland surface fire spread modelling, 1990–2007. 3: Simulation and mathematical analogue models. *Int. J. Wildland Fire* **2009**, *18*, 387–403. [[CrossRef](#)]
- Sullivan, A.; Sharples, J.; Matthews, S.; Plucinski, M. A downslope fire spread correction factor based on landscape-scale fire behaviour. *Environ. Model. Softw.* **2014**, *62*, 153–163. [[CrossRef](#)]
- Fernandes, P.M.; Botelho, H.S.; Rego, F.C.; Loureiro, C. Empirical modelling of surface fire behaviour in maritime pine stands. *Int. J. Wildland Fire* **2009**, *18*, 698–710. [[CrossRef](#)]
- Rossa, C.G.; Fernandes, P.M. Empirical Modeling of Fire Spread Rate in No-Wind and No-Slope Conditions. *For. Sci.* **2018**, *64*, 358–370. [[CrossRef](#)]
- Minsavage-Davis, C.D.; Davies, G.M. Evaluating the Performance of Fire Rate of Spread Models in Northern-European *Calluna vulgaris* Heathlands. *Fire* **2022**, *5*, 46. [[CrossRef](#)]
- Curry, J.R.; Fons, W.L. Forest-fire behavior studies. *Mech. Eng.* **1940**, *62*, 219–225.

17. Mell, W.; Jenkins, M.A.; Gould, J.; Cheney, P. A physics-based approach to modelling grassland fires. *Int. J. Wildland Fire* **2007**, *16*, 1–22. [[CrossRef](#)]
18. Simeoni, A.; Salinesi, P.; Morandini, F. Physical modelling of forest fire spreading through heterogeneous fuel beds. *Int. J. Wildland Fire* **2011**, *20*, 625–632. [[CrossRef](#)]
19. Balbi, J.-H.; Morandini, F.; Silvani, X.; Filippi, J.-B.; Rinieri, F. A physical model for wildland fires. *Combust. Flame* **2009**, *156*, 2217–2230. [[CrossRef](#)]
20. Hilton, J.; Sullivan, A.; Swedosh, W.; Sharples, J.; Thomas, C. Incorporating convective feedback in wildfire simulations using pyrogenic potential. *Environ. Model. Softw.* **2018**, *107*, 12–24. [[CrossRef](#)]
21. Grishin, A.M.; Matvienko, O.V.; Rudi, Y.A. Mathematical simulation of the formation of heat tornadoes. *J. Eng. Phys.* **2008**, *81*, 897–904. [[CrossRef](#)]
22. Grishin, A.M.; Yakimov, A.S. Mathematical modeling of the wood ignition process. *Thermophys. Aeromechanics* **2013**, *20*, 463–475. [[CrossRef](#)]
23. Rothermel, R.C. *A Mathematical Model for Predicting Fire Spread in Wildland Fuels*; Research Paper; USDA Intermountain Forest and Range Experiment Station: Ogden, UT, USA, 1972; Volume 115, p. 40. Available online: <https://srs.fs.usda.gov/pubs/32533> (accessed on 10 July 2022).
24. Andrews, P.L.; Cruz, M.; Rothermel, R.C. Examination of the wind speed limit function in the Rothermel surface fire spread model. *Int. J. Wildland Fire* **2013**, *22*, 959–969. [[CrossRef](#)]
25. Ascoli, D.; Vacchiano, G.; Motta, R.; Bovio, G. Building Rothermel fire behaviour fuel models by genetic algorithm optimisation. *Int. J. Wildland Fire* **2015**, *24*, 317–328. [[CrossRef](#)]
26. Trunfio, G.A.; D’Ambrosio, D.; Rongo, R.; Spataro, W.; Di Gregorio, S. A New Algorithm for Simulating Wildfire Spread through Cellular Automata. *ACM Trans. Model. Comput. Simul.* **2011**, *22*, 1–26. [[CrossRef](#)]
27. Jiang, W.; Wang, F.; Fang, L.; Zheng, X.; Qiao, X.; Li, Z.; Meng, Q. Modelling of wildland-urban interface fire spread with the heterogeneous cellular automata model. *Environ. Model. Softw.* **2021**, *135*, 104895. [[CrossRef](#)]
28. Karafyllidis, I.; Thanailakis, A. A model for predicting forest fire spreading using cellular automata. *Ecol. Model.* **1997**, *99*, 87–97. [[CrossRef](#)]
29. Gharakhanlou, N.M.; Hooshangi, N. Dynamic simulation of fire propagation in forests and rangelands using a GIS-based cellular automata model. *Int. J. Wildland Fire* **2021**, *30*, 652–663. [[CrossRef](#)]
30. Alexandridis, A.; Russo, L.; Vakalis, D.; Bafas, G.V.; Siettos, C.I. Wildland fire spread modelling using cellular automata: Evolution in large-scale spatially heterogeneous environments under fire suppression tactics. *Int. J. Wildland Fire* **2011**, *20*, 633–647. [[CrossRef](#)]
31. Trucchia, A.; D’Andrea, M.; Baghino, F.; Fiorucci, P.; Ferraris, L.; Negro, D.; Gollini, A.; Severino, M. PROPAGATOR: An Operational Cellular-Automata Based Wildfire Simulator. *Fire* **2020**, *3*, 26. [[CrossRef](#)]
32. Rothermel, R.C.; Wilson, R.A.; Morris, G.A.; Sackett, S.S. *Modeling Moisture Content of Fine Dead Wildland Fuels: Input to the BEHAVE Fire Prediction System*; Research Paper; USDA Forest Service Intermountain Research Station: Ogden, UT, USA, 1986; Volume 359. Available online: <https://www.srs.fs.usda.gov/pubs/33476> (accessed on 10 July 2022).
33. Frost, S.M.; Alexander, M.E.; Jenkins, M.J. The Application of Fire Behavior Modeling to Fuel Treatment Assessments at Army Garrison Camp Williams, Utah. *Fire* **2022**, *5*, 78. [[CrossRef](#)]
34. Catchpole, E.A.; Mestre, N.J.d.; Gill, A.M. Intensity of fire at its perimeter. *Aust. For. Res.* **1982**, *12*, 47–54.
35. Andrews, P.L. *The Rothermel Surface Fire Spread Model and Associated Developments: A Comprehensive Explanation*; USDA Forest Service Rocky Mountain Research Station: Fort Collins, CO, USA, 2018. Available online: <https://www.srs.fs.usda.gov/pubs/55928> (accessed on 10 July 2022). [[CrossRef](#)]
36. Finney, M.A. *FARSITE: Fire Area Simulator—Model Development and Evaluation*; Research Paper; USDA Forest Service Rocky Mountain Forest and Range Experiment Station: Fort Collins, CO, USA, 1998. [[CrossRef](#)]
37. Finney, M.A. A computational method for optimising fuel treatment locations. *Int. J. Wildland Fire* **2007**, *16*, 702–711. [[CrossRef](#)]
38. Vichniac, G.Y. Simulating physics with cellular automata. *Phys. D Nonlinear Phenom.* **1984**, *10*, 96–116. [[CrossRef](#)]
39. Adou, J.; Billaud, Y.; Brou, D.; Clerc, J.-P.; Consalvi, J.-L.; Fuentes, A.; Kaiss, A.; Nmira, F.; Porterie, B.; Zekri, L.; et al. Simulating wildfire patterns using a small-world network model. *Ecol. Model.* **2010**, *221*, 1463–1471. [[CrossRef](#)]
40. Li, X.; Zhang, M.; Zhang, S.; Liu, J.; Sun, S.; Hu, T.; Sun, L. Simulating Forest Fire Spread with Cellular Automation Driven by a LSTM Based Speed Model. *Fire* **2022**, *5*, 13. [[CrossRef](#)]
41. Finney, M.A. Fire growth using minimum travel time methods. *Can. J. For. Res.* **2002**, *32*, 1420–1424. [[CrossRef](#)]
42. Zhang, Y.; Feng, Z.D.; Tao, H.; Wu, L.; Li, K.; Xin, D. Simulating wildfire spreading processes in a spatially heterogeneous landscapes using an improved cellular automaton model. In Proceedings of the IGARSS 2004. 2004 IEEE International Geoscience and Remote Sensing Symposium, Anchorage, AK, USA, 20–24 September 2004.
43. Roeva, O.; Vassilev, P.; Ikonov, N.; Marinov, P.; Zoteva, D.; Atanassova, V.; Tsakov, H. MkbGFire Software—An Example of Game Modelling of Forest Fires in Bulgaria. In *Uncertainty and Imprecision in Decision Making and Decision Support: New Challenges, Solutions and Perspectives*; Springer International Publishing: Cham, Switzerland, 2021.
44. Erdős, P. Graph Theory and Probability. *Can. J. Math.* **2018**, *11*, 34–38. [[CrossRef](#)]
45. Bondy, J.A.; Murty, U.S.R. *Graph Theory with Applications*; Macmillan: London, UK, 1976; Volume 290.
46. Breedveld, P. Multibond graph elements in physical systems theory. *J. Frankl. Inst.* **1985**, *319*, 1–36. [[CrossRef](#)]

47. Cetinkaya, E.K.; Alenazi, M.J.; Cheng, Y.; Peck, A.M.; Sterbenz, J.P. On the fitness of geographic graph generators for modelling physical level topologies. In Proceedings of the 2013 5th International Congress on Ultra Modern Telecommunications and Control Systems and Workshops (ICUMT), Almaty, Kazakhstan, 10–13 September 2013.
48. Fowler, R.J.; Little, J.J. Automatic extraction of Irregular Network digital terrain models. In Proceedings of the 6th Annual Conference on Computer Graphics and Interactive Techniques, Chicago, IL, USA, 8–10 August 1979; Association for Computing Machinery: New York, NY, USA, 1979; pp. 199–207.
49. Leri, M.M. Forest fire on a configuration graph with random fire propagation. *Inform. Ee Primen.* **2015**, *9*, 65–71.
50. Leri, M.; Pavlov, Y. Forest Fire Models on Configuration Random Graphs. *Fundam. Informaticae* **2016**, *145*, 313–322. [[CrossRef](#)]
51. Messinger, M.E. Firefighting on the triangular grid. *J. Comb. Math. Comb. Comput.* **2007**, *63*, 37–45.
52. Gordinowicz, P. Planar graph is on fire. *Theor. Comput. Sci.* **2015**, *593*, 160–164. [[CrossRef](#)]
53. Wang, W.; Kong, J. Surviving rate of graphs and Firefighter Problem. *Adv. Math.* **2021**, *50*, 1–21. [[CrossRef](#)]
54. Johnston, P.; Kelso, J.; Milne, G.J. Efficient simulation of wildfire spread on an irregular grid. *Int. J. Wildland Fire* **2008**, *17*, 614–627. [[CrossRef](#)]
55. Stepanov, A.; Smith, J.M. Modeling wildfire propagation with Delaunay triangulation and shortest path algorithms. *Eur. J. Oper. Res.* **2012**, *218*, 775–788. [[CrossRef](#)]
56. Hajian, M.; Melachrinoudis, E.; Kubat, P. Modeling wildfire propagation with the stochastic shortest path: A fast simulation approach. *Environ. Model. Softw.* **2016**, *82*, 73–88. [[CrossRef](#)]
57. Penney, G.; Habibi, D.; Cattani, M.; Carter, M. Calculation of Critical Water Flow Rates for Wildfire Suppression. *Fire* **2019**, *2*, 3. [[CrossRef](#)]
58. Abdel-Hamid, O.; Mohamed, A.R.; Jiang, H.; Deng, L.; Penn, G.; Yu, D. Convolutional neural networks for speech recognition. *IEEE/ACM Trans. Audio Speech Lang. Process.* **2014**, *22*, 1533–1545. [[CrossRef](#)]
59. He, K.; Zhang, X.; Ren, S.; Sun, J. Deep Residual Learning for Image Recognition. In Proceedings of the 2016 IEEE Conference on Computer Vision and Pattern Recognition (CVPR), Las Vegas, NV, USA, 27–30 June 2016.
60. Vaswani, A.; Shazeer, N.; Parmar, N.; Uszkoreit, J.; Jones, L.; Gomez, A.N.; Kaiser, Ł.; Polosukhin, I. Attention is all you need. In Proceedings of the 31st International Conference on Neural Information Processing Systems, Long Beach, CA, USA, 4–9 December 2017; Curran Associates Inc.: New York, NY, USA, 2017; pp. 6000–6010.
61. Allaire, F.; Mallet, V.; Filippi, J.-B. Emulation of wildland fire spread simulation using deep learning. *Neural Netw.* **2021**, *141*, 184–198. [[CrossRef](#)]
62. Hodges, J.L.; Lattimer, B.Y. Wildland Fire Spread Modeling Using Convolutional Neural Networks. *Fire Technol.* **2019**, *55*, 2115–2142. [[CrossRef](#)]
63. Pfaff, T.; Fortunato, M.; Sanchez-Gonzalez, A.; Battaglia, P.W. Learning Mesh-Based Simulation with Graph Networks. *arXiv* **2021**, arXiv:2010.03409.
64. Sanchez-Gonzalez, A.; Godwin, J.; Pfaff, T.; Ying, R.; Leskovec, J.; Battaglia, P. Learning to simulate complex physics with graph networks. In Proceedings of the 37th International Conference on Machine Learning, ICML 2020, Virtual, 13–18 July 2020; International Machine Learning Society (IMLS): Princeton, NJ, USA, 2020.
65. Guo, X.; Li, W.; Iorio, F. Convolutional neural networks for steady flow approximation. In Proceedings of the 22nd ACM SIGKDD International Conference on Knowledge Discovery and Data Mining, KDD 2016, San Francisco, CA, USA, 13–17 August 2016; Association for Computing Machinery: New York, NY, USA, 2016.
66. Rumelhart, D.E.; Hinton, G.E.; Williams, R.J. Learning representations by back-propagating errors. *Nature* **1986**, *323*, 533–536. [[CrossRef](#)]
67. Hecht, N. Theory of the backpropagation neural network. In Proceedings of the International 1989 Joint Conference on Neural Networks, Washington, DC, USA, 18–22 June 1989.
68. LeCun, Y.; Boser, B.; Denker, J.; Henderson, D.; Howard, R.; Hubbard, W.; Jackel, L. Handwritten digit recognition with a back-propagation network. In Proceedings of the 2nd International Conference on Neural Information Processing Systems; MIT Press: Cambridge, MA, USA, 1989; pp. 396–404.
69. Yosinski, J.; Clune, J.; Bengio, Y.; Lipson, H. How transferable are features in deep neural networks? *Adv. Neural Inf. Process. Syst.* **2014**, *2*, 3320–3328.
70. Sze, V.; Chen, Y.-H.; Yang, T.-J.; Emer, J.S. Efficient Processing of Deep Neural Networks: A Tutorial and Survey. *Proc. IEEE* **2017**, *105*, 2295–2329. [[CrossRef](#)]
71. Samek, W.; Montavon, G.; Lapuschkin, S.; Anders, C.J.; Müller, K.-R. Explaining Deep Neural Networks and Beyond: A Review of Methods and Applications. *Proc. IEEE* **2021**, *109*, 247–278. [[CrossRef](#)]
72. LAFD. Getty Fire. 2019. Available online: <https://www.lafd.org/news/getty-fire> (accessed on 10 July 2022).
73. LANDFIRE. About Usgs Landfire. 2022. Available online: <https://www.landfire.gov/about.php> (accessed on 10 July 2022).
74. USGS. What is GeoMAC. 2022. Available online: <https://wildfire.usgs.gov/geomac/GeoMACTransition.shtml> (accessed on 10 July 2022).
75. Utah, U.o. Weather Conditions for KVVY 2020. Available online: https://mesowest.utah.edu/cgi-bin/droman/meso_base_dyn.cgi?product=&past=1&stn=KVVY&unit=0&time=LOCAL&day1=29&month1=10&year1=2019&hour1=1 (accessed on 9 January 2020).

76. Zigner, K.; Carvalho, L.M.V.; Peterson, S.; Fujioka, F.; Duine, G.-J.; Jones, C.; Roberts, D.; Moritz, M. Evaluating the Ability of FARSITE to Simulate Wildfires Influenced by Extreme, Downslope Winds in Santa Barbara, California. *Fire* **2020**, *3*, 29. [[CrossRef](#)]
77. Hao, Y. *California Wildfire Spread Prediction Using FARSITE and the Comparison with the Actual Wildfire Maps Using Statistical Methods*; UCLA Electronic Theses and Dissertations: Los Angeles, CA, USA, 2018. Available online: <https://escholarship.org/uc/item/8nz6p4hc> (accessed on 10 July 2022).
78. Minaee, S.; Boykov, Y.Y.; Porikli, F.; Plaza, A.J.; Kehtarnavaz, N.; Terzopoulos, D. Image Segmentation Using Deep Learning: A Survey. *IEEE Trans. Pattern Anal. Mach. Intell.* **2022**, *44*, 3523–3542. [[CrossRef](#)]
79. Barber, C.B.; Dobkin, D.P.; Huhdanpaa, H. The quickhull algorithm for convex hulls. *ACM Trans. Math. Softw.* **1996**, *22*, 469–483. [[CrossRef](#)]
80. Lee, D.T.; Schachter, B.J. Two algorithms for constructing a Delaunay triangulation. *Int. J. Parallel Program.* **1980**, *9*, 219–242. [[CrossRef](#)]
81. Zhou, T.; Ding, L.; Ji, J.; Yu, L.; Wang, Z. Combined estimation of fire perimeters and fuel adjustment factors in FARSITE for forecasting wildland fire propagation. *Fire Saf. J.* **2020**, *116*, 103167. [[CrossRef](#)]
82. Radočaj, D.; Jurišić, M.; Gašparović, M. A wildfire growth prediction and evaluation approach using Landsat and MODIS data. *J. Environ. Manag.* **2022**, *304*, 114351. [[CrossRef](#)]
83. Tan, L.; de Callafon, R.A.; Block, J.; Crawl, D.; Çağlar, T.; Altıntaş, I. Estimation of wildfire wind conditions via perimeter and surface area optimization. *J. Comput. Sci.* **2022**, *61*, 101633. [[CrossRef](#)]
84. Mandel, J.; Beezley, J.D.; Kochanski, A.K. Coupled atmosphere-wildland fire modeling with WRF 3.3 and SFIRE 2011. *Geosci. Model Dev.* **2011**, *4*, 591–610. [[CrossRef](#)]
85. Ramirez, J.; Monedero, S. Wildfire Analyst User’s Guide: The Different Simulation Modes. 2022. Available online: http://www.wildfireanalyst.com/help/english/?reverse_mode.htm (accessed on 10 July 2022).
86. LANDFIRE. LANDFIRE Data Viewer. 2022. Available online: <https://www.landfire.gov/viewer/> (accessed on 17 August 2022).
87. LANDFIRE. Landscape (lcp) Files. 2022. Available online: <https://landfire.gov/lcp.php> (accessed on 17 August 2022).
88. Ioffe, S.; Szegedy, C. Batch normalization: Accelerating deep network training by reducing internal covariate shift. In Proceedings of the 32nd International Conference on International Conference on Machine Learning, Lille, France, 6–11 July 2015; JMLR: Lille, France, 2015; Volume 37, pp. 448–456.
89. Glorot, X.; Bordes, A.; Bengio, Y. Deep Sparse Rectifier Neural Networks. In Proceedings of the Fourteenth International Conference on Artificial Intelligence and Statistics, Fort Lauderdale, FL, USA, 11–13 April 2011.
90. Lecun, Y.; Bottou, L.; Bengio, Y.; Haffner, P. Gradient-based learning applied to document recognition. *Proc. IEEE* **1998**, *86*, 2278–2324. [[CrossRef](#)]
91. Mount, J. The Equivalence of Logistic Regression and Maximum Entropy Models. 2011. Available online: <https://win-vector.com/2011/09/23/the-equivalence-of-logistic-regression-and-maximum-entropy-models/> (accessed on 17 August 2022).
92. Campbell, M.J.; Dennison, P.E.; Thompson, M.P.; Butler, B.W. Assessing Potential Safety Zone Suitability Using a New Online Mapping Tool. *Fire* **2022**, *5*, 5. [[CrossRef](#)]
93. Campbell, M.J.; Page, W.G.; Dennison, P.E.; Butler, B.W. Escape Route Index: A Spatially-Explicit Measure of Wildland Firefighter Egress Capacity. *Fire* **2019**, *2*, 40. [[CrossRef](#)]